Published in final edited form as:
J Neural Eng. 2013 June ; 10(3): 036009. doi:10.1088/1741-2560/10/3/036009.

The Response of Retinal Neurons to High-Frequency Stimulation

Changsi Cai[1,2,3,4], **Perry Twyford**[1,3], and **Shelley Fried**[1,3]

[1]VA Boston Healthcare System, Boston, MA

[2]School of Biomedical Engineering, Shanghai Jiao-Tong University, Shanghai, China

[3]Department of Neurosurgery, Massachusetts General Hospital and Harvard Medical School, Boston, MA

[4]Center of Functionally Integrative Neuroscience (CFIN), Aarhus University, Aarhus, Denmark

Abstract

Objective—High-rate pulse trains have proven to be effective in cochlear prosthetics and, more recently, have been shown to elicit a wide range of interesting response properties in axons of the PNS. Surprisingly, the effectiveness of such trains for use in retinal prostheses has not been explored.

Approach—Using cell-attached patch clamp methods, we measured the *in vitro* response of two rabbit retinal ganglion cell (RGC) types, OFF-Brisk Transient (OFF-BT) and ON-OFF Directionally Selective (DS), to trains of biphasic pulses delivered at 2000 pulses per second (PPS).

Main Results—For OFF-BT cells, response onset occurred at ~20 uA, and maximum response occurred at ~40 uA. Interestingly, spiking levels *decreased* for further increases in amplitude. In contrast, DS cells had a spiking onset at ~25 uA and maintained strong spiking as stimulus amplitude was increased, even at the highest levels tested. Thus, a low-amplitude stimulus train at 2000 PPS (~25 μA) will activate OFF-BT cells strongly, while simultaneously activating DS cells only weakly. In contrast, a high amplitude train (~75 μA) will activate DS cells strongly while suppressing responses in OFF-BT cells.

Significance—The response differences between cell types suggest some forms of preferential activation may be possible, and further testing is warranted. Further, the scope of the response differences found here suggests activation mechanisms that are more complex than those described in previous studies.

Keywords

Retinal prosthesis; Electric stimulation; Ganglion cells; Initial segment

1. Introduction

In recent years, there have been several significant advancements towards the goal of restoring vision in blind patients using retinal prosthetics [1–5] (for review, see [6]). For example, subjects with both sub-retinal and epi-retinal devices can perform simple visual tasks including identification of shapes [2, 5], basic navigation [7, 8] and some subjects can

Corresponding Author: Shelley I. Fried, PhD, Massachusetts General Hospital / Harvard Medical School, 185 Cambridge Street – Simches 3824, Boston, MA 02114, fried.shelley@mgh.harvard.edu.

Disclosures
No conflicts of interest, financial or otherwise, are declared by the author(s).

even read simple words made up of large, high-contrast letters [5, 9, 10]. While these advancements represent important milestones in the quest for prosthetic vision, clinical results are still far from perfect. For example, 44.8 –100.3 seconds are required on average for patients to read a single letter [10], suggesting that patients use the information from the prosthetic to infer information about each letter, rather than conventional 'reading' as is performed by those with normal sight. To increase the performance of retinal prosthetic devices, several important challenges should be addressed. Many of the engineering challenges, such as increasing the number and density of the stimulating electrodes and improving the computing power necessary for data processing, are expected to be solved in the near future as advances in processing speed and microfabrication techniques continue to occur [11–13]. Other challenges, such as forming a better understanding of how electrical stimulation affects the retinal response, require further research [13–20]. For example, many elements of the natural neural code of the retina are still not well understood [21–26]. Additionally, the ability to create specific patterns of neural activity via electrical stimulation, or even to understand the patterns of neural activity that are created, remains limited. To address these challenges, it is important to continue to investigate the retinal response to electric stimulation, and to develop novel stimulation strategies. Stimulation paradigms that can more accurately recreate the natural retinal firing patterns are likely to lead to improved prosthetic vision, and increased patient quality of life.

The spiking patterns that arise during normal vision are highly complex [27]. For example, at least twelve different types of retinal ganglion cells (RGCs) [28–31] each extract different features of the visual world and use distinct patterns of action potentials to transmit these features to higher visual centers [31–34]. The ideal prosthetic would re-create these patterns with perfect fidelity, as this would result in the highest quality of vision. However, perfect fidelity would require simultaneous creation of different spike patterns in many closely situated RGCs – technology that is currently beyond the capabilities of existing devices. Nevertheless, the ability to preferentially activate even one or two types of RGCs might significantly improve the quality of elicited vision. For example, if ON cells could be activated without simultaneously activating OFF cells, or midget cells could be activated without simultaneously activating parasol cells, key elements of normal retinal processing could be re-created, presumably leading to higher quality vision.

Previous studies have shown that the sensitivity to electric stimulation is different for different types of RGCs [35, 36]. For example, the threshold for direct activation of the local edge detector (LED) was nearly 5x greater than that of the brisk transient (BT) when single 100 μs cathodal pulses were used [35]. These differences are thought to arise because of differences in the distribution of voltage-gated sodium (and other) ion channels within the axon initial segment (AIS), the site thought to mediate the response to electric stimulation [35]. Unfortunately, the differences from these single pulse stimulation studies are probably too small to be of practical use.

Additional response differences across types are revealed when trains of pulses are used to stimulate RGCs [14, 37–39]. For example, nearly all RGC types respond with one spike to each pulse in the train at rates up to 100 pulses per second (PPS). However, only a few types can 'follow' rates of 200 PPS, and only BT cells can follow even faster rates [39]. It is somewhat interesting that the cell types that can follow faster pulse rates are the ones that generate high rates of spiking in response to light stimuli, while those types that normally respond more sluggishly to light can only follow lower pulse rates. Thus, a high-rate pulse train delivered to a heterogeneous population of neurons would elicit a high-rate burst of spikes in those types that normally respond with high rates, while simultaneously eliciting more sluggish responses in those types that normally respond sluggishly. It remains to be determined whether any clinical benefit is associated with this sort of approach.

It is interesting to consider whether even faster rates of stimulation might enhance the response differences described above, as the highest stimulus rates evaluated with retinal neurons has been limited to a few hundred PPS. In contrast, rates of 2000–5000 PPS have been used in the cochlear prosthetic [40–42], where they are known to effectively modulate the activity of auditory nerve fibers. In addition, high rate pulse trains (rates ranging from 5 to 50 kHz) can also elicit robust neural activity in the PNS [43]. Interestingly however, increasing the amplitude of stimulation in the PNS converts activation into an effective block of spike transmission [43–46]. The threshold for the onset of blockade is dependent on both stimulus rate and the type of axon, e.g. the sensitivity of myelinated fibers is different from that of unmyelinated [43, 46]. Importantly, the sensitivity profiles of myelinated vs. non-myelinated fibers are offset sufficiently such that at one stimulus rate, myelinated fibers can be blocked while non-myelinated fibers are not; the opposite was true at a higher stimulus rate [43]. This is an important finding because it suggests that separate neural pathways can be independently manipulated.

The mechanism underlying conduction block may arise from differences in the distribution or kinetics of voltage-gated ion channels between different axon types [45]. Therefore, because the distribution and kinetics of ion channels in RGCs is variable across types, the possibility arises that different types of RGCs may have different sensitivities to high rates of stimulation. Here, we examine the response of two different types of RGC to 2000 PPS stimulation in a rabbit model. We found that the steady state response of each RGC type was different. Although further study is required, this stimulation paradigm may lead to improved selectivity of individual RGC types. Portions of the work presented here have been described previously [47].

2. Methods

2.1. Animal preparation and retina isolation

The care and use of animals followed all federal and institutional guidelines and all protocols were approved by the Institutional Animal Care and Use Committees of the Boston VA Healthcare System and/or the Subcommittee of Research Animal Care of the Massachusetts General Hospital. New Zealand white rabbits (~2.5 kg) were anesthetized with injections of xylazine/ketamine and subsequently euthanized with an intracardial injection of sodium pentobarbital. Immediately after death, the eyes were removed. All procedures following eye removal were performed under dim red illumination. The front of the eye was removed, the vitreous was eliminated, and the eye cup dissected so that the retina could be flattened. The retina was separated from the retinal pigment epithelium and mounted, photoreceptor side down, to a 10 mm square piece of Millipore filter paper (0.45 μm HA Membrane Filter) that was mounted with vacuum grease to the recording chamber (~1.0 ml volume). A 2 mm circle in the center of the Millipore paper allowed light from below to be projected on to the photoreceptors.

2.2. Light responses and electrophysiology

Patch pipettes were used to make small holes in the inner limiting membrane and RGCs were targeted under visual control. Spiking was recorded with a loose, cell-attached patch electrode (5–6 MΩ), filled with Ames medium. Two silver-chloride coated silver wires served as the ground; each was positioned approximately 8 mm from the targeted cell and approximately 6 mm from each other.

The light stimulus and data acquisition software was controlled by custom software written in LabView (National Instruments) and Matlab (Mathworks) and written by G. Spor, T. Muench, and D. Balya. The electric stimulation software was written by D. Freeman. The sampling rate of the data acquisition setup was 100 kHz, and the time resolution of the

stimulus generator was 50 kHz. Light stimuli were projected onto the retina from below through a liquid crystal display projector (Dell) and focused onto the outer segments of the photoreceptors. A photopic background intensity was maintained throughout the experiment (~4 nW/m^2) [1]. Light stimuli consisted of stationary flashed squares (size range: 100–1,000 μm), 1 s duration, centered at the soma and moving bars (300 × 1,800 μm moving at 600 μm/s in two orthogonal directions).

Two types of ganglion cells were used in this study: OFF-Brisk Transient (n = 16) and ON-OFF Directionally Selective (n = 6). Initial studies of the response to 2000 PPS stimulation were performed in BT cells while subsequent studies in DS cells allowed response differences across types to be identified. These two types were chosen because they can be identified with high accuracy via response to light stimulus. Cells were classified as brisk transient/alpha cells (BT) if they responded with high frequency and transient bursts of spiking to stimuli centered in their receptive field [1, 4, 5]. Consistent with previous reports, responses were largest for larger squares and were typically small or nonexistent for small squares (≤100 μm). Similar to previous studies, we found both ON and OFF varieties of these cells, however only OFF-BT cells were used in this study. Cells were classified as directionally selective (DS) if their response to the flashed 200-μm square was ON–OFF and if their response to back-and-forth motion of the bars was directional, e.g., spiking levels were considerably higher in one direction versus the other [48]. These cells are more accurately classified as ON–OFF DS cells to distinguish them from a different type of DS cell that generates responses only at light luminance increases (ON DS cells). Although ON-OFF DS cells only were studied here, they are sometimes referred to in the manuscript as ‘DS’.

2.3. Electric Stimulation

Electric stimulation was delivered via a 10 kΩ Platinum-Iridium electrode (MicroProbes); the exposed area was conical with an approximate height of 125 μm and base diameter of 15 μm, giving a surface area of ~5,900 μm^2, comparable to a 40 μm disk electrode. Two silver chloride electrodes in the bath served as the ground. The height of the stimulating electrode remained fixed at 25 μm above the inner limiting membrane; the distance was calibrated by touching the surface of the inner limiting membrane with the tip of the electrode and then using the micromanipulator to raise the height by 25 μm. Pulse stimuli were controlled by Multi-Channel Systems STG2004 hardware and software. The stimulating electrode was placed directly over the sodium-channel band on the proximal axon - this has been shown to correspond to the center of the region with the lowest threshold and is generally centered between 20 and 60 μm from the soma along the proximal axon [13]. Using an iterative process, we were able to quickly find the center of the low-threshold region: movement of the stimulating electrode towards the center of the low-threshold region resulted in decreasing thresholds while movement away from the center resulted in increasing thresholds. We used the location of lowest stimulation threshold as the approximate center of the sodium-channel band.

2.4. Stimuli

Pulsatile stimuli were biphasic pulses (equal and opposite rectangular phases, cathodal first) delivered at rates of 2000 PPS. Cathodal and anodal phase durations were 100 μs each, with 150 μs between phases. Prior to stimulation, the threshold for activation was first determined at 10 PPS. For this rate, the phase duration remained 100 μs, but the interval between cathodal and anodal phase onsets was 10 ms. Threshold was defined as the stimulus level necessary to elicit a spike for one-half of pulses delivered at 10 PPS; amplitudes were delivered in multiples of T. The cells used in this study did not exhibit spontaneous firing and therefore all recorded spikes were assumed to be stimulus induced.

2.5. Exponential Fits

Spike histograms were fit using a double exponential equation, shown below.

$$y = P_{ss} + \underbrace{P_{fast} * e^{-\frac{x}{\tau_{fast}}}}_{\text{Fast Component}} + \underbrace{P_{slow} * e^{-\frac{x}{\tau_{slow}}}}_{\text{Slow Component}} \quad (1)$$

The double exponential fit consists of P_{ss}, or the steady state firing rate of the cell, and both a fast and slow component, with corresponding time constants. Error was determined using the standard equation for Root Mean Squared Error.

$$RMSE = \sqrt{\frac{1}{n}\sum_{i=1}^{n}(Data_i - Fit_i)^2} \quad (2)$$

2.6. Gaussian Fits

ISI histograms were visually inspected to see if they contained two peaks (bursting) or one peak (non-bursting). Peaks were fit independently with the general equation for a Gaussian curve, shown below,

$$y = a * e^{-\frac{(x-b)^2}{2*c^2}} \quad (3)$$

Where a is the peak height, b is the peak center, and c corresponds to the peak width.

3. Results

We measured the response of retinal ganglion cells (RGCs) to 5-second trains of pulsatile stimulation delivered at 2000 pulses per second (PPS, methods. Testing was initially confined to a single type of ganglion cell known as OFF-Brisk Transient (OFF-BT) (Methods), in order to eliminate potential response differences that can arise when different types of RGCs are activated by extracellular electric stimulation. After the response to 2000 PPS stimulation in these cells was assessed, a second phase of testing in a different type of RGC (Directionally Selective, DS) was performed, allowing the differences in response to be analyzed.

Responses to 2000 PPS stimuli were complex (Figure 1). Raw waveforms (Figure 1a, middle) typically consisted of artifacts at regularly spaced intervals that were precisely correlated with the pattern of cathodic and anodic pulses (Figure 1a, top). For some portions of the response however, there were distortions in the regular pattern of artifacts (Figure 1a bottom). We speculated that these distortions arose as the result of spikes that had been elicited, but confirmation of this supposition was difficult from visual observation alone. In order to subtract the stimulation artifact computationally, the portion of the raw waveform from 0.1 ms immediately preceding the onset of each cathodal waveform to 0.15 ms following the offset of the same pulse was extracted for each cathodal pulse (Figure 1b, left). Overlay of all extracted portions for the response from Figure 1a is shown in Figure 1b (left); the numerical average (of all extracted portions) was used to represent the average cathodal artifact and is indicated in red. Prior preliminary inspection of the raw waveform suggested that only a small percentage of pulses elicited spikes, and therefore the calculation of the average artifact would be distorted only a small amount (by elicited spikes). The average anodal artifact was determined in a similar manner (Figure 1b, right).

The average artifacts (anodal and cathodal) were subtracted from each corresponding location of the raw waveform to yield a filtered version of the raw response (Figure 1c). Spike timing was determined by cross-correlating the filtered raw response (Figure 1c, left) with the average light-elicited action potential (Figure 1c, right). The cross-correlation yielded a series of peaks (Figure 1d) - the timing of each corresponded to the onset of an elicited action potential. Overlay of all individual action potentials extracted in this manner (Figure 1e) revealed that elicited spikes were highly consistent in form, and closely resembled the light-elicited action potential.

Because current thresholds are known to vary, even within a single ganglion cell sub-type, we ran a series of preliminary experiments to gauge the approximate threshold of each cell tested. Pulses were applied at 10 PPS because the lower rate allows direct visualization of elicited spikes, making it easier to quickly assess efficacy. Trains were applied at 10 PPS over a range of amplitudes in order to determine the amplitude for which 50% of pulses elicited spikes. This level was referred to as ‘T’ and was used as a baseline level for testing at 2000 PPS, e.g. stimulus amplitudes at 2000 PPS were 2*T, 3*T, etc. The values of T ranged from 12 to 30 (mean: 19.20 ± 7.25 μA) in the 9 OFF-BT cells for which it was measured.

Similar to previous studies using lower stimulus rates [14, 37–39], the spiking patterns elicited by 2000 PPS stimulation (Figure 2a) were influenced by both intrinsic properties of the cell (and/or the presynaptic circuitry) as well as the properties of the stimulus. For example, responses were strong immediately following onset of the pulse train (arrows in Figure 2a), but became weaker over the 5-second time course, suggesting that OFF-BT cells become desensitized to 2000 PPS stimulation. The initial 250 ms responses for each amplitude level are shown in expanded time scale in the right panel. The strong initial decrease in spike rate (arrows in Figure 2b) coupled with a more gradual decrease in response over time, suggests that more than one desensitizing mechanism may be involved in the response. The amplitude of stimulation was also seen to influence the responses. For example, the number of elicited spikes varied with stimulus strength (Figure 2b). Interestingly, there was a decrease in the number of spikes elicited at higher stimulus amplitudes. Another influence of amplitude was the way elicited spikes clustered together at some amplitude levels but not at others (Figure 2a, compare responses to 1.5*T and 3*T). These differences did not arise from cellular run-down or some other type of fatigue, as responses remained consistent throughout the duration of an experiment (Figs. 2c, d). We explore these response properties in more detail in the sections below.

3.1. Desensitization to 2000 PPS stimulation

To explore the desensitization of the OFF-BT response over time, we binned spikes (response to 3*T of a typical cell is shown in Figure 3a) into 50 ms bins (Figure 3b) (each bin count in Figure 3b is the average of 3 repeats). Responses typically declined sharply over the first few bins and then declined more gradually over the duration of the pulse train. Consistent with this observation, a double exponential curve (solid line) provided a better fit to the bin counts than a single exponential. For the data in Figure 3b, error values (Methods) were 41% higher for the single exponential curve than the double exponential. Double exponentials provided a better fit than single exponentials in >91% of trials. The time-constants associated with the two exponentials, the fast and slow components, were 5.82 ± 1.47 ms and 3.12 ± 1.49 s (respectively) and did not vary significantly with stimulus amplitude (Figure 3c). The presence of both fast and slow modes of desensitization observed here are reminiscent of the two modes of desensitization observed in response to slower rates of longer-pulse stimulation (designed to activate the synaptic network) [49]. Although the exact values of the time constants found here are different from those of the previous study (~176 ms and 14 s for fast and slow, respectively [49]), the qualitative similarity raises

the possibility that 2000 PPS stimulation activates RGCs indirectly, e.g. the observed spiking responses are secondary to activation of bipolar cells, or perhaps even photoreceptors. Activation through the synaptic network would be somewhat surprising however, as short duration pulses are typically thought to activate ganglion cells directly.

To determine the site(s) of activation, we pharmacologically blocked excitatory synaptic input to RGCs by adding 6-cyano-7-nitroquinoxaline-2,3-dione (CNQX, 50μM) and DL-2-amino-7-phosphonoheptanoic acid (AP7, 100μM) to the perfusion bath (Figure 4). Surprisingly, there was no significant change to the responses in the presence of these blockers (n=3) – either in the general appearance of the responses (left panels) or when histograms of the ISIs were compared (right). Therefore the responses to 2000 PPS stimulation arise through direct activation of the RGC and are not secondary to activation of one or more of the neurons that deliver excitatory synaptic input to RGCs. This finding was consistent for all stimulus amplitude levels tested.

3.2. Response sensitivity to amplitude

The qualitative inspection of Figures 2a & b revealed notable differences between the responses arising from the different levels of stimulus amplitude, including the strength of the response as well as the arrangement of spikes into bursts. Response strength vs. amplitude was studied further by plotting the total number of spikes elicited from a single cell (averaged over 3 trials) as a function of amplitude (Figure 5a). As expected, a relatively small number of spikes were elicited at the lowest amplitude (1*T). Spike counts increased as amplitude was increased to 1.5*T and increased further at 2*T, but surprisingly the count began to decrease as amplitude increased above 2*T. Further increases in amplitude led to a progressive reduction in total spike count. This pattern was consistent across the population of OFF-BT cells tested (n=9): all cells demonstrated the strongest response at intermediate amplitudes (1.5-3*T), and a decreased response at higher amplitudes – Figure 5b contains an overlay of all OFF-BT cells and confirms that the level of elicited spiking was influenced strongly by stimulus amplitude. The plot also reveals that the maximum response occurred at mid-range amplitudes in all cells: responses were strongest at 1.5*T, 2*T and 3*T for 2, 5 and 1 cells respectively. Finally, it was interesting to note that the steady state rate of spiking (spiking after the initial burst) was quite low for the highest amplitudes (Discussion).

Because the rate at which spikes were elicited at the onset of 2000 PPS stimulation was generally larger than the steady state rate (Figs. 2a, b), we isolated the initial portion of the response in order to analyze its sensitivity to changes in amplitude – independent of the rest of the response. This was done by determining the number of spikes elicited within the first 100 ms for each amplitude level (Figure 5c, solid line). Spike counts increased rapidly as a function of amplitude for amplitudes < 2*T but increased much more gradually for amplitudes > 2*T. The response curve did not change qualitatively when the duration associated with the ‘initial portion’ of the response was increased to either 200 or 300 ms (Figure 5c, dashed and light lines, respectively). This result has two important implications. First, because the spike counts for the full 5-second duration exhibited a decrease at higher amplitude levels while the initial portion of the response did not exhibit a decrease, it confirms that the decreases in spike levels at higher amplitudes (Figure 5a) arise because the steady state spiking level is reduced. Second, it also suggests that if only a short window of the response is considered, the spiking output reaches maximum levels at relatively low stimulus amplitude levels and remains steady at higher amplitude levels.

3.3. Inter-spike Interval Analysis

Because burst spiking has previously been shown to arise through indirect activation [20, 37], it was unusual that we observed bursting that occurred while synaptic input was

blocked. To better characterize the response patterns to 2000 PPS stimulation, we explored how the inter-spike intervals (ISIs) of the responses varied with stimulus amplitude. This provided a simple way to examine the properties of elicited spike bursts, which appeared at some amplitude levels (e.g. Figure 2a, 1–2*T) but not others (Figure 2a, 3–5*T). To quantify these differences, histograms of the ISIs for all spikes in each pulse train were generated (Figure 6).

To minimize the effect arising from the initial burst of spikes that arose at the onset of each pulse train (Figure 2a, arrows), we only included those spikes that occurred 250 ms after stimulus onset. The peaks of the ISI histograms were generally restricted to two regions: one occurred at very low ISIs (~3 ms) and was narrow (hereafter referred to as the short-ISI peak) while the other peak was centered at ISIs of >10 ms and was considerably wider than the first peak (hereafter referred to as the long-ISI peak). The short ISI-peak arises from spikes within bursts, while the long-ISI peak corresponds to the interval between successive bursts. We calculated the center of each peak (or a Gaussian curve fit to that peak (Methods)) as the approximate ISI average for that peak. Figure 7a plots the center of all short-ISI peaks as a function of stimulus amplitude for all cells, and reveals that burst responses were elicited primarily by amplitude levels in the low to middle part of our range. For example, at 1.5*T and 2*T, 9/9 and 8/9 cells elicited bursts, respectively, whereas only 1/9 cells elicited bursts at either 4*T or 5*T.

Peak locations across all cells and amplitudes ranged from 2.63 to 3.87 ms, suggesting that the interval between spikes was fairly consistent across the range of cells and amplitudes. The mean ISI of the spikes in these bursts (horizontal lines) increased from 2.98 ± 0.30 to 3.29 ± 0.17 as amplitude increased from 1*T to 1.5*T ($p=0.02$, paired t-test) and then increased further to 3.43 ± 0.22 ($p=0.01$, paired t-test) as amplitude increased to 2*T. These increases in ISI with increasing stimulus amplitude were somewhat surprising as we had originally expected higher amplitude stimuli to be *more* effective, and therefore associated with shorter latencies.

The second peak in the ISI histogram was centered at a larger ISI (>10 ms) and was also broader than the short interval peak. This peak was thought to be a measure of the intervals between bursts and, consistent with this notion, occurred for only those combinations of cells and amplitudes in which bursts were readily observable (Figure 7b). Note that while responses for 1*T often exhibited bursting, the inter-burst interval was irregular so a long-ISI peak was not observed. The average of the peak centers decreased as stimulus amplitude increased from 1.5*T to 2*T and from 2*T to 3*T (1.5*T: 28.03 ± 9.03, 2*T: 20.36 ± 7.46, 3*T: 18.17 ± 5.57, $p=0.05$, one-way ANOVA) suggesting that the interval between bursts is also a function of amplitude. Responses to amplitudes ≥ 4*T did not exhibit burst-like clustering and the ISI profiles were correspondingly sparse.

3.4. Spike Waveform Analysis

To explore the factors contributing to the increase in ISIs with pulse amplitude, we examined the kinetics of spike waveforms at each level. Interestingly, we found that the depolarizing portion of the action potential varied with the amplitude of the stimulus (Figure 8a, c). Spikes arising from amplitudes ≤ 2*T exhibited two phases of depolarization (n=9/9) - the approximate onset of each phase (see below) is indicated by the dashed vertical lines in Figure 8a and reveals a small depolarization that occurs prior to a larger depolarization. The early depolarization was not observed in response to stimulus amplitudes ≥3*T.

The presence of two depolarizing phases in the action potential has been described previously in RGCs as well as in a wide array of other neurons [39, 50, 51]. In these previous studies, the early phase was shown to correspond to the somatic depolarization

arising when an action potential was generated within the AIS and the second, larger phase corresponds to the subsequent somatic spike. Results from several recent studies using electric stimulation indicate that the sodium channel band within the axon initial segment (AIS) is the site of spike initiation in response to extracellular electric stimulation [13, 35, 48, 52], and therefore the possibility exists that the two phases of depolarization observed in the present study correspond to the same two phases observed in physiological studies, i.e. the early phase we observed corresponds to the somatic depolarization arising when an action potential is generated within the AIS and the second, larger phase corresponds to the subsequent somatic spike. Because two phases of depolarization were observed only for stimulus amplitudes ≤2*T, our results further suggest that the spike is initiated in the band only for low amplitude levels of 2000 PPS stimulation. At higher amplitudes the spike may be initiated directly in the soma.

Overlay of the average action potential elicited at each amplitude (Figure 8c) revealed that the delay between the first phase (onset of the band spike) and the second phase (onset of the somatic spike) increased as amplitude increased from 1*T to 2*T. We calculated the difference by determining the approximate onset of each phase of depolarization using the second derivative of the spike waveform (Figure 8b) (Methods); the local minima of the second derivative at the onset of each phase were used as the onset time (indicated by dashed vertical lines in Figs. 8a/b). For the cell of Figure 8, the latency between band spike and somatic spike was 0.19 ms, 0.26 ms and 0.38 ms for amplitudes of 1, 1.5 and 2*T, respectively (Figure 8a). For the population, latencies were 0.17 ± 0.01 ms, 0.25 ± 0.06 ms and 0.37 ± 0.11 ms for 1, 1.5 and 2*T (respectively).

The distance between the AIS and the soma in rabbit BT cells is 26.9 ± 5.5 μm [35]. The length of the sodium channel band in these same cells is 40.6 ± 5.39 μm and computer simulations suggest that the action potential is initiated in the distal portion of the band. Thus, the distance the action potential traverses from band to soma is estimated to be approximately 67 μm. The delays that we observed between the onset of the band spike and the onset of the somatic spike varied from 0.19–0.38 ms which corresponds to action potential propagation velocities of between 0.2 and 0.3 m/s. This range of velocity is much slower than recent measurements of axonal propagation velocity made in portions of the proximal axon of the rabbit retina (1.3 ±0.3 m/s) [53]. It is not clear how to resolve this discrepancy. One possibility is that the first depolarizing phase observed here does not in fact correspond to the onset of an action potential within the sodium channel band. Another potential explanation is that antidromic and orthodromic propagation velocities differ, possibly due to the tapered shape of the axon initial segment [35]. It is interesting, however, that this slow propagation velocity between the sodium channel band and the soma has been reported outside the retina; direct physiological measurements made in hippocampal mossy fibers showed propagation speeds from AIS to soma of 0.24 m/s [54]. Further study is needed to investigate this issue.

The increase in latency with increasing stimulus amplitude is also intriguing. It seems unlikely that the passive propagation properties of this portion of the axon are changing, and therefore suggests that either the band spike itself is getting weaker, or its effectiveness in initiating the somatic spike is reduced. This first possibility is consistent with our finding that at high amplitudes (≥3*T) the depolarization arising from the band spike was too small to be measured, perhaps because it was not even initiated. A single (large) phase of depolarization further suggests that at such amplitudes, the action potential may be initiated directly in the soma. These findings are also consistent with the ISI increases seen in Figure 7a. As the delay between band spike and somatic spike increases (from 1*T to 2*T), the RGC cannot spike as quickly, resulting in an increase in the location of the short-ISI peak.

We also examined the correlation between the onset of spiking and the phase of the stimulus pulse. A peri-stimulus time histogram (PSTH) was created at each amplitude level for the initial (AIS) depolarization and separately for the second, larger (somatic) depolarization (Figure 8a, middle and right columns, respectively). The PSTH of the initial phase of depolarization, presumably corresponding to the onset of the AIS spike, formed a single peak that was centered ~0.25 ms after the onset of the anodal phase. The timing of this peak was consistent at all amplitude levels for which the initial depolarization was observed. In contrast, the latency between the onset of the anodal phase of the stimulus pulse and the onset of the second phase of depolarization (corresponding to the somatic spike) varied with amplitude, increasing from ~0.4 ms at 1*T to ~0.6 ms at 2*T. At amplitude levels ≥ 3*T, there was little correlation between stimulus phase and spike onset.

3.5. Responses in DS cells

Because previous studies with electric stimulation have shown that different types of RGCs can exhibit different sensitivities to slower rates of pulsatile stimulation [35, 39], we measured the responses to 2000 PPS stimulation in a second type of ganglion cell: the ON-OFF Directionally Selective (DS) ganglion cell (Figure 9). Many components of the response were qualitatively similar to the responses from OFF-BT cells. For example, fewer spikes were generated at the lowest amplitudes, responses decayed with both a fast and slow component, and burst spiking was observed at some amplitudes (1.5*T) but not others (3*T).

The most notable difference between DS and OFF-BT cells was the relatively strong spiking level that persisted at amplitude levels ≥ 60 μA in DS cells (Figure 9c). Similar to the analysis for OFF-BT cells, we determined the average number of total spikes elicited as a function of stimulus level for DS cells (Figure 9c, solid line) and found that, in contrast to the responses of OFF-BT cells, the total spike counts did not decrease as amplitude exceeded 2*T. Overlay of the average DS and OFF-BT responses, scaled to the average current levels, allows the responses of the two cell types to be directly compared. Interestingly, the overlay suggests that it may be possible to activate each of the two cell types independently with 2000 PPS stimulation. At high amplitude levels, i.e. 100 μA (solid vertical line), the steady response of the OFF-BT cell is small while the steady state response of the DS cells is large. The opposite is true at lower stimulus levels, i.e. 30 μA (dashed vertical line): OFF-BT cells generate a large response while DS cells are mostly quiet. When the first 100 ms of the responses of DS cells was examined (analogous to Figure 5c), sensitivity to amplitude was large for levels ≤ 2*T and minimal for levels above 2*T (inset, solid line). Comparison to the response from OFF-BT cells (dotted line) indicates that OFF-BT cells reach maximum spike levels before DS cells (Discussion).

One other notable difference between DS cells and OFF-BT cells arose from the ISIs associated with bursts (Figure 10). The short-ISI peak locations for DS cells were larger than those for OFF-BT cells (compare Figure 10A with Figure 7A), suggesting that spikes occur more rapidly in BT bursts than in the bursts of DS cells. Interestingly, the mean short-ISI peak location for DS cells decreased as amplitude increased from 1 to 2*T – opposite to the effect seen in OFF-BT cells. The inter-burst interval decreased as amplitude increased (Figure 10b) – similar to the effect seen in OFF-BT cells.

4. Discussion

The primary goal of this study was to explore whether high rates of stimulation, similar to the rates used in other neural prosthetic applications [40–42], could be used to activate retinal neurons. We found that although RGCs were responsive to 2000 PPS stimulation, sensitivity was confined to a relatively narrow range of amplitudes. In addition, the strength

of the response was less than that elicited by lower rates of stimulation, e.g. 200–600 PPS [39]. We also found that different types of RGCs had different thresholds, as well as different sensitivities to stimulus amplitude. These differences offer the possibility that individual types of RGCs can be selectively activated, although further development will be required to bring this to fruition. The response differences did not arise from presynaptic neurons or circuitry, suggesting instead that they arise from one or more components within the ganglion cell itself. Previous computational studies suggest that the threshold differences to single pulses across types arise from relatively simple anatomical differences, e.g. the length and/or location of the band of voltage-gated sodium channels within the axon initial segment [52]. However, it is unlikely that these same anatomical differences can account for some of the response differences observed here, e.g. the biphasic response profile of one cell type but not the other. Instead it is likely that differential expression of specific sub-types of voltage-gated sodium channels and/or other types of voltage-gated channels underlie such response differences. Further testing will be required to uncover these specifics. While only OFF-BT and ON-OFF DS cells are examined in the present study, future work will investigate the responses of other cell types to high-frequency electrical stimulation.

4.1. Amplitude sensitivity

Ganglion cell responses to 2000 PPS stimulation were highly sensitive to stimulation amplitude. In OFF-BT cells, the number of spikes elicited increased as the amplitude of the pulse train increased from 1 to 2*T (about 20 to 40 μA). However, as amplitude increased further, the number of elicited spikes decreased (Figure 5). At 4*T and 5*T the number of elicited spikes was quite low – comparable to the counts elicited by 1*T. It is surprising that OFF-BT responses were suppressed at high amplitudes given that earlier studies using lower rates report only monotonic increases in spiking with amplitude [39]. For the ON-OFF DS ganglion cell, the number of spikes elicited also increased with amplitude from 1*T until about 2*T (about 25 to 50 μA). However, for this cell type spike levels remained approximately constant as amplitude increased further to 5*T (Figure 9). This sensitivity to amplitude of 2000 PPS stimulation was similar to the DS cells' response to lower rates of stimulation.

The differences in response between the two cell types suggest that a limited level of selective activation may be achievable. For example, at low amplitudes (~30 μA) 2000 PPS stimulation generated strong responses in OFF-BT cells while generating only weak responses in DS cells. In contrast, prolonged trains of 2000 PPS stimulation at high amplitudes (~100 μA) suppressed the responses in OFF-BT cells while generating robust activity in DS cells. The ability to selectively activate individual types of RGCs is of considerable interest, especially if the two primary RGC types of the human retina (midget and parasol) can be selectively targeted, as this would allow more physiologically realistic patterns of neural activity to be created with the prosthesis. However, since measurements of the responses of *in vitro* RGCs to natural scenes suggest that the neural code of the retina consists of sparse bursts of spikes [32], the ability to suppress OFF-BT responses with the prolonged trains of pulses used in this study may be of only limited clinical use. Nevertheless, stimulus rates considerably higher than 2000 PPS have been used effectively in other applications [40–46], raising the possibility that enhanced selectivity can be achieved with other stimulus parameters, e.g. changes in the waveform or rate of the stimulus.

Other neural prosthetic applications might benefit greatly from the ability to selectively suppress one or more specific types of neurons. For example, bladder voiding in spinal cord injury patients can be optimized by a stimulus that relaxes the external urethral sphincter at the same time the bladder is compressed. This creates the need for a stimulus waveform that can suppress the pudendal nerve. Consistent with our results, Boger et. al. found improved

voiding of the bladder in cats when the pudendal nerve was activated at 2000 PPS [55], suggesting that the suppression observed here does not arise from properties unique to OFF-BT ganglion cells. Understanding which properties of the neuron underlie the observed suppression may help us to predict which types of neural populations will be suppressed by 2000 PPS stimulation and which will not.

4.2. Response mechanism to 2000 PPS stimulation

In response to a single stimulus pulse, the threshold differences measured across RGC types are thought to arise from specific differences in the anatomy of each type. For example, differences in the curvature of the axon as it emerges from the soma, differences in the length and/or location of the band of voltage-gated sodium channels within the axon initial segment, and differences in the size of the soma have all been shown to influence threshold [35, 52]. However, the biphasic profile of amplitude sensitivity observed here has not been reported in any of these studies, making it unlikely that the suppression of OFF-BT cells observed at high frequencies arises from any of the differences listed above. Computer models that explored the sensitivity of axons to high rates of stimulation found a response suppression that could be explained by the Hodgkin-Huxley type kinetics of voltage-gated sodium channels within the axon or by the kinetics of voltage-gated potassium channels [44, 56]. This raises the possibility that the suppression of spiking observed in OFF-BT but not DS cells at high frequencies arises because of differences in the types of sodium channels (each with different kinetics) and/or differences in other types of voltage-gated ion channels across the two types. Improved understanding of the specific cellular elements that influence the response to stimulation might help to identify stimulus parameters that maximize the response differences between types, thereby improving the ability for selective activation. Importantly, our results also suggest that the temporal dynamics of voltage-gated ion channels should be incorporated into all simulations in which the response to electric stimulation is evaluated.

4.3. Is 2000 PPS stimulation effective?

The number of spikes elicited by 2000 PPS stimulation was less than the number that could be elicited by lower stimulation rates. For example, even at ‘optimum’ amplitude (~2*T), the number of spikes elicited by OFF-BT cells in response to 2000 PPS pulse trains never exceeded 200 for any one-second period (Figure 5). At these amplitudes, one spike was only elicited for roughly every 5–10 pulses. The limitation in rate was not a function of the cell itself since many of these same cells generated one spike per pulse in response to 500 PPS, i.e. the cells were capable of firing at least 500 spikes per second (data not shown, but see [39]). The reduced level of firing in response to 2000 PPS stimulation was not unique to OFF-BT cells, as the maximum number of spikes elicited in one second in DS cells was ~80 (Figure 9) while such cells can elicit counts as high as 200 (in response to 200 PPS stimulation). Thus, at first glance our results could suggest that the total number of spikes that can be generated by stimulation at 2000 PPS is less than the totals that can be generated by rates in the 200–500 PPS range. However, the higher levels of spiking elicited by the lower rates were achieved only at higher amplitude levels (e.g. 10*T), and equal-amplitude comparison (2*T vs. 2*T) of the spike counts elicited by 500 PPS and 2000 PPS stimulation were similar. This suggests that the effectiveness of the two rates is in fact similar. Nevertheless, one of the key differences between the responses to 2000 PPS stimulation and the responses to lower rates is the relative insensitivity of ganglion cells to high amplitudes of 2000 PPS. The responses to 2000 PPS, in which one spike is elicited every few pulses, is reminiscent of the “Gildemeister Effect”, in which successive high frequency stimuli are summed together, each pushing the membrane closer to threshold [57, 58].

4.4. Response desensitization

Firing rates were generally highest at the onset of the pulse train and decayed rapidly for a brief period following stimulus onset. A more gradual decay continued throughout the duration of the stimulus (Figs. 3, 9). Consistent with this observation, the decay in spike rate was best fit with a double exponential (5.82 ms and 3.12 s for the fast and slow time constants, respectively). Because pharmacological blockage of synaptic input did not alter the responses to 2000 PPS stimulation (Figure 4), our results suggest that the accommodative processes that underlie the changes in rate are mediated entirely within the ganglion cell. It is interesting to note that the decay in spike rate seen here resembles the decays observed by Freeman et. al. (fast and slow time constants of 176 ms and 14 s, respectively) in response to slower rates (2–16 PPS) of 1.0 ms pulses [49]. Their stimuli were designed to activate presynaptic neurons and so the decay (in their study) was thought to arise, at least in part, from one or more of the mechanisms associated with synaptic transmission, e.g. depletion of neurotransmitter at bipolar cell terminals, desensitization of the synaptic receptors on the dendrites of RGCs, etc. However, because we found that mechanisms intrinsic to the ganglion cell have decay rates similar to those from the Freeman study, the possibility exists that the accommodative processes observed in their study also originate entirely within the ganglion cell. If so, the time constants associated with accommodation may be similar for a wide array of stimulus waveforms. Consistent with this notion, the two components of desensitization found here and in the Freeman study are similar to the two phases of brightness fading reported in human subjects during clinical trials [59], suggesting that the clinical phenomenon may arise from a physiological reduction in RGC spiking.

4.5. Burst responses

Much previous work has shown that when burst spiking arises in response to electric stimulation, it is due to indirect activation of the ganglion cell, i.e. spiking is secondary to activation of one or more neurons that deliver presynaptic input to the ganglion cell [20, 37]. Thus, our observation of bursts that were insensitive to pharmacological blockade of synaptic input was somewhat surprising; testing at all stimulus levels revealed that responses to 2000 PPS stimulation were always mediated via direct activation of the ganglion cell. The properties of the bursts that arise through indirect activation are thought to be shaped by the strength with which presynaptic neurons are activated: strongly activated presynaptic cells lead to larger and more prolonged releases of excitatory neurotransmitter, which in turn leads to longer and stronger spike bursts [37, 60, 61].

Somewhat surprisingly, this same relationship did not hold true for bursts seen in OFF BT cells in the present study. For example, we found that inter-spike intervals generally increased with increasing stimulus amplitude (Figs 7) suggesting that in contrast to indirect activation, the effectiveness with which bursts are generated by 2000 PPS stimulation decreases with the amplitude of the stimulus pulse. Burst spiking was not elicited at all amplitude levels but interestingly, those amplitudes for which it was were the same as those in which the spike waveform contained two separate phases (Fig. 8). This raises the possibility that burst generation is mediated within the AIS, but further work will be needed to confirm this. The interval between the onsets of the first and second depolarization phases was found to lengthen with increases in the amplitude of the stimulus train (Fig. 8) suggesting the possibility that the efficiency/strength of the AIS spike is reduced with increased amplitude. It is unclear what causes this reduction in efficiency but it is possible that it arises from an inhibitory element within the AIS (i.e. a potassium channel [62]) that is dormant at lower amplitudes but becomes activated at higher amplitudes. Other properties of the bursts, e.g. the intervals between bursts as well as the factors that mediate both the onset

and offset of bursts, were also sensitive to amplitude. The factors that shape these properties were not revealed in this study and are worthy of further investigation.

Acknowledgments

This work was funded in part by the VA Boston Healthcare System (1 I01RX000350) and the NIH (1 R01EY019967-01)

References

1. Humayun MS, et al. Visual perception elicited by electrical stimulation of retina in blind humans. Arch Ophthalmol. 1996; 114(1):40–6. [PubMed: 8540849]
2. Humayun MS, et al. Visual perception in a blind subject with a chronic microelectronic retinal prosthesis. Vision Res. 2003; 43(24):2573–81. [PubMed: 13129543]
3. Yanai D, et al. Visual performance using a retinal prosthesis in three subjects with retinitis pigmentosa. Am J Ophthalmol. 2007; 143(5):820–827. [PubMed: 17362868]
4. Rizzo JF 3rd, et al. Perceptual efficacy of electrical stimulation of human retina with a microelectrode array during short-term surgical trials. Invest Ophthalmol Vis Sci. 2003; 44(12): 5362–9. [PubMed: 14638739]
5. Zrenner E, et al. Blind Retinitis Pigmentosa Patients Can Read letters and Recognize the Direction of Fine Stripe Patterns With Subretinal Electronic Implants. Invest Ophthalmol Vis Sci. 2009; 50:Abstract #4581.
6. Weiland JD, Cho AK, Humayun MS. Retinal prostheses: current clinical results and future needs. Ophthalmology. 2011; 118(11):2227–37. [PubMed: 22047893]
7. Ahuja AK. Blind subjects implanted with the Argus II retinal prosthesis are able to improve performance in a spatial-motor task. Br J Ophthalmol. 2011; 95:539–543. [PubMed: 20881025]
8. Barry MP, Dagnelie G. Use of the Argus II Retinal Prosthesis to Improve Visual Guidance of Fine Hand Movements. Invest Ophthalmol Vis Sci. 2012
9. Zrenner E, et al. Subretinal electronic chips allow blind patients to read letters and combine them to words. Proc Biol Sci. 2011; 278(1711):1489–97. [PubMed: 21047851]
10. daCruz L, et al. Patients Blinded by Outer Retinal Dystrophies Are Able to Identify Letters Using the Argus II Retinal Prosthesis System. Invest Ophthalmol Vis Sci. 2010; 51(E-Abstract):Abstract #: 2023.
11. Palanker D, et al. Design of a high-resolution optoelectronic retinal prosthesis. J Neural Eng. 2005; 2(1):S105–20. [PubMed: 15876646]
12. Weiland J, et al. Progress towards a high-resolution retinal prosthesis. Conf Proc IEEE Eng Med Biol Soc. 2005; 7:7373–5. [PubMed: 17281984]
13. Sekirnjak C, et al. High-resolution electrical stimulation of primate retina for epiretinal implant design. J Neurosci. 2008; 28(17):4446–56. [PubMed: 18434523]
14. Sekirnjak C, et al. Electrical stimulation of mammalian retinal ganglion cells with multielectrode arrays. J Neurophysiol. 2006; 95(6):3311–27. [PubMed: 16436479]
15. Stett A, Mai A, Herrmann T. Retinal charge sensitivity and spatial discrimination obtainable by subretinal implants: key lessons learned from isolated chicken retina. J Neural Eng. 2007; 4(1):S7–16. [PubMed: 17325418]
16. Margalit E, Thoreson WB. Inner retinal mechanisms engaged by retinal electrical stimulation. Invest Ophthalmol Vis Sci. 2006; 47(6):2606–12. [PubMed: 16723477]
17. Stasheff SF. Emergence of Sustained Spontaneous Hyperactivity and Temporary Preservation of OFF Responses in Ganglion Cells of the Retinal Degeneration (rd1) Mouse. J Neurophysiol. 2008; 99(3):1408–21. [PubMed: 18216234]
18. Ye JH, Goo YS. The slow wave component of retinal activity in rd/rd mice recorded with a multi-electrode array. Physiol Meas. 2007; 28(9):1079–88. [PubMed: 17827655]
19. Jensen RJ, Rizzo JF 3rd. Responses of ganglion cells to repetitive electrical stimulation of the retina. J Neural Eng. 2007; 4(1):S1–6. [PubMed: 17325407]

20. Jensen RJ, Ziv OR, Rizzo JF. Responses of rabbit retinal ganglion cells to electrical stimulation with an epiretinal electrode. J Neural Eng. 2005; 2(1):S16–21. [PubMed: 15876650]
21. Cao X, Merwine DK, Grzywacz NM. Dependence of the retinal Ganglion cell's responses on local textures of natural scenes. J Vis. 2011; 11(6)
22. Felsen G, Dan Y. A natural approach to studying vision. Nat Neurosci. 2005; 8(12):1643–6. [PubMed: 16306891]
23. Geisler WS. Visual perception and the statistical properties of natural scenes. Annu Rev Psychol. 2008; 59:167–92. [PubMed: 17705683]
24. Mante V, et al. Independence of luminance and contrast in natural scenes and in the early visual system. Nat Neurosci. 2005; 8(12):1690–7. [PubMed: 16286933]
25. Puchalla JL, et al. Redundancy in the population code of the retina. Neuron. 2005; 46(3):493–504. [PubMed: 15882648]
26. Simoncelli EP, Olshausen BA. Natural image statistics and neural representation. Annu Rev Neurosci. 2001; 24:1193–216. [PubMed: 11520932]
27. Masland RH. The fundamental plan of the retina. Nat Neurosci. 2001; 4(9):877–86. [PubMed: 11528418]
28. Rockhill RL, et al. The diversity of ganglion cells in a mammalian retina. J Neurosci. 2002; 22(9): 3831–43. [PubMed: 11978858]
29. DeVries SH, Baylor DA. Mosaic arrangement of ganglion cell receptive fields in rabbit retina. Journal of Neurophysiology. 1997; 78(4):2048–2060. [PubMed: 9325372]
30. Roska B, Werblin F. Vertical interactions across ten parallel, stacked representations in the mammalian retina. Nature. 2001; 410(6828):583–587. [PubMed: 11279496]
31. O'Brien BJ, et al. Intrinsic physiological properties of cat retinal ganglion cells. J Physiol. 2002; 538(Pt 3):787–802. [PubMed: 11826165]
32. Meister M, Berry MJ 2nd. The neural code of the retina. Neuron. 1999; 22(3):435–50. [PubMed: 10197525]
33. Meister M, Lagnado L, Baylor DA. Concerted Signaling by Retinal Ganglion-Cells. Science. 1995; 270(5239):1207–1210. [PubMed: 7502047]
34. Schnitzer MJ, Meister M. Multineuronal firing patterns in the signal from eye to brain. Neuron. 2003; 37(3):499–511. [PubMed: 12575956]
35. Fried SI, et al. Axonal sodium-channel bands shape the response to electric stimulation in retinal ganglion cells. J Neurophysiol. 2009; 101(4):1972–87. [PubMed: 19193771]
36. Jensen RJ, Rizzo JF 3rd. Activation of retinal ganglion cells in wild-type and rd1 mice through electrical stimulation of the retinal neural network. Vision Res. 2008; 48(14):1562–8. [PubMed: 18555890]
37. Fried SI, Hsueh HA, Werblin FS. A method for generating precise temporal patterns of retinal spiking using prosthetic stimulation. J Neurophysiol. 2006; 95(2):970–8. [PubMed: 16236780]
38. Ahuja AK, et al. An In Vitro Model of a Retinal Prosthesis. IEEE Trans Biomed Eng. 2008; 55(6): 1744–53. [PubMed: 18714839]
39. Cai C, et al. Response variability to high rates of electric stimulation in retinal ganglion cells. J Neurophysiol. 2011; 106(1):153–62. [PubMed: 21490287]
40. Litvak L, Delgutte B, Eddington D. Auditory nerve fiber responses to electric stimulation: modulated and unmodulated pulse trains. J Acoust Soc Am. 2001; 110(1):368–79. [PubMed: 11508961]
41. Litvak LM, Delgutte B, Eddington DK. Improved temporal coding of sinusoids in electric stimulation of the auditory nerve using desynchronizing pulse trains. J Acoust Soc Am. 2003; 114(4 Pt 1):2079–98. [PubMed: 14587607]
42. Litvak LM, et al. Desynchronization of electrically evoked auditory-nerve activity by high-frequency pulse trains of long duration. J Acoust Soc Am. 2003; 114(4 Pt 1):2066–78. [PubMed: 14587606]
43. Joseph L, Butera RJ. High-frequency stimulation selectively blocks different types of fibers in frog sciatic nerve. IEEE Trans Neural Syst Rehabil Eng. 2011; 19(5):550–7. [PubMed: 21859632]

44. Kilgore KL, Bhadra N. Nerve conduction block utilising high-frequency alternating current. Med Biol Eng Comput. 2004; 42(3):394–406. [PubMed: 15191086]
45. Bhadra N, Kilgore KL. Direct current electrical conduction block of peripheral nerve. IEEE Trans Neural Syst Rehabil Eng. 2004; 12(3):313–24. [PubMed: 15473193]
46. Bhadra N, et al. Simulation of high-frequency sinusoidal electrical block of mammalian myelinated axons. J Comput Neurosci. 2007; 22(3):313–26. [PubMed: 17200886]
47. Fried, SI.; Cai, C.; Ren, Q. High frequency electric stimulation of retinal neurons elicits physiological signaling patterns. Conf Proc IEEE Eng Med Biol Soc; 2011; 2011. p. 1077-80.
48. Behrend MR, et al. Selective labeling of retinal ganglion cells with calcium indicators by retrograde loading in vitro. J Neurosci Methods. 2009; 179(2):166–72. [PubMed: 19428523]
49. Freeman DK, Fried SI. Multiple components of ganglion cell desensitization in response to prosthetic stimulation. J Neural Eng. 2011; 8(1):016008. [PubMed: 21248379]
50. Stuart G, Schiller J, Sakmann B. Action potential initiation and propagation in rat neocortical pyramidal neurons. J Physiol. 1997; 505(Pt 3):617–32. [PubMed: 9457640]
51. Carras PL, Coleman PA, Miller RF. Site of action potential initiation in amphibian retinal ganglion cells. J Neurophysiol. 1992; 67(2):292–304. [PubMed: 1569462]
52. Jeng J, et al. The sodium channel band shapes the response to electric stimulation in retinal ganglion cells. J Neural Eng. 2011; 8(3):036022. [PubMed: 21558602]
53. Zeck G, Lambacher A, Fromherz P. Axonal transmission in the retina introduces a small dispersion of relative timing in the ganglion cell population response. PLoS One. 2011; 6(6):e20810. [PubMed: 21674067]
54. Schmidt-Hieber C, Jonas P, Bischofberger J. Action potential initiation and propagation in hippocampal mossy fibre axons. J Physiol. 2008; 586(7):1849–57. [PubMed: 18258662]
55. Boger A, Bhadra N, Gustafson KJ. Bladder voiding by combined high frequency electrical pudendal nerve block and sacral root stimulation. Neurourol Urodyn. 2008; 27(5):435–9. [PubMed: 18041769]
56. Liu H, et al. The role of slow potassium current in nerve conduction block induced by high-frequency biphasic electrical current. IEEE Trans Biomed Eng. 2009; 56(1):137–46. [PubMed: 19224727]
57. Gildemeister M. Untersuchungen über die wirkung der mittelfrequenzströme auf den menschen. Pflugers Arch. 1944; 247:366–404.
58. Gildemeister M. Zur theorie des elektrischen reizes, V: polarisation durch wechselstrome. Ber Sachs Ges Wiss. 1930; 81:303–313.
59. Perez Fornos A, et al. Temporal properties of visual perception on electrical stimulation of the retina. Invest Ophthalmol Vis Sci. 2012; 53(6):2720–31. [PubMed: 22447863]
60. Stett A, et al. Electrical multisite stimulation of the isolated chicken retina. Vision Res. 2000; 40(13):1785–95. [PubMed: 10814763]
61. Jensen RJ, Ziv OR, Rizzo JF 3rd. Thresholds for activation of rabbit retinal ganglion cells with relatively large, extracellular microelectrodes. Invest Ophthalmol Vis Sci. 2005; 46(4):1486–96. [PubMed: 15790920]
62. Van Wart A, Trimmer JS, Matthews G. Polarized distribution of ion channels within microdomains of the axon initial segment. J Comp Neurol. 2007; 500(2):339–52. [PubMed: 17111377]

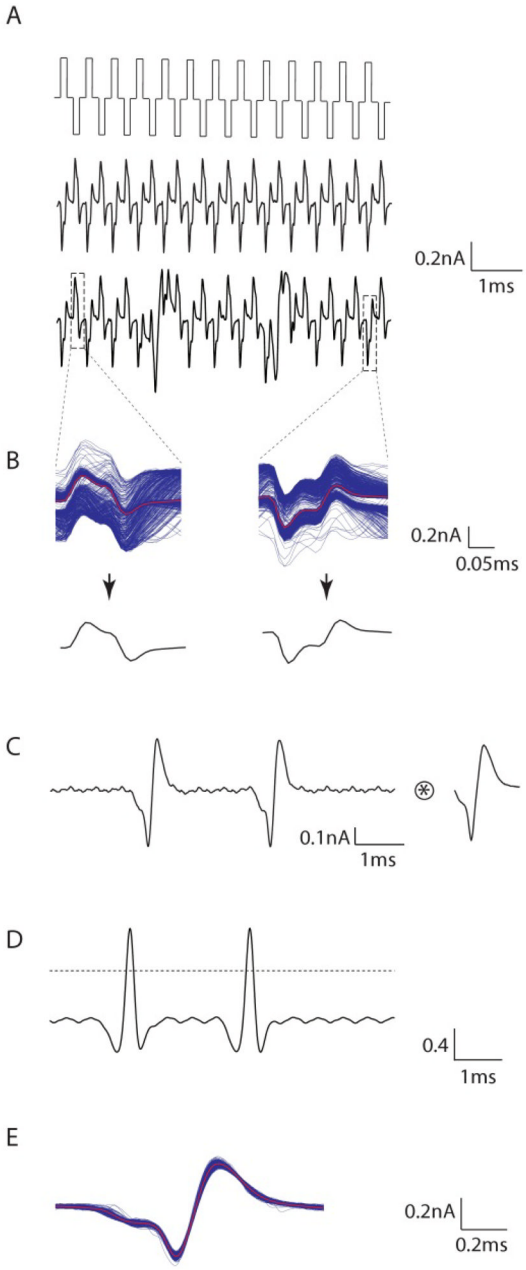

Figure 1.

2000 PPS stimulation elicits action potentials. (A) Biphasic stimuli at 2000 PPS (top) elicit a periodic response (middle) in OFF-BT RGCs that was phase-locked to the stimulus. Irregularities in the periodicity pattern (bottom) were hypothesized to be the result of elicited action potentials. (B) Cathodal and anodal artifacts (top) were averaged over the entire trial (bottom), and then subtracted from the corresponding location in the raw waveform to yield a filtered waveform (C), in which action potentials, similar in size and shape to light-elicited action potentials (right), were readily apparent. (D) The filtered waveform was cross-correlated with the average light elicited action potential (top), and peaks in the cross-correlation (bottom) were used to determine the timing of each action potential. (E) Overlay of all extracted action potentials from a single trial. Red: average waveform.

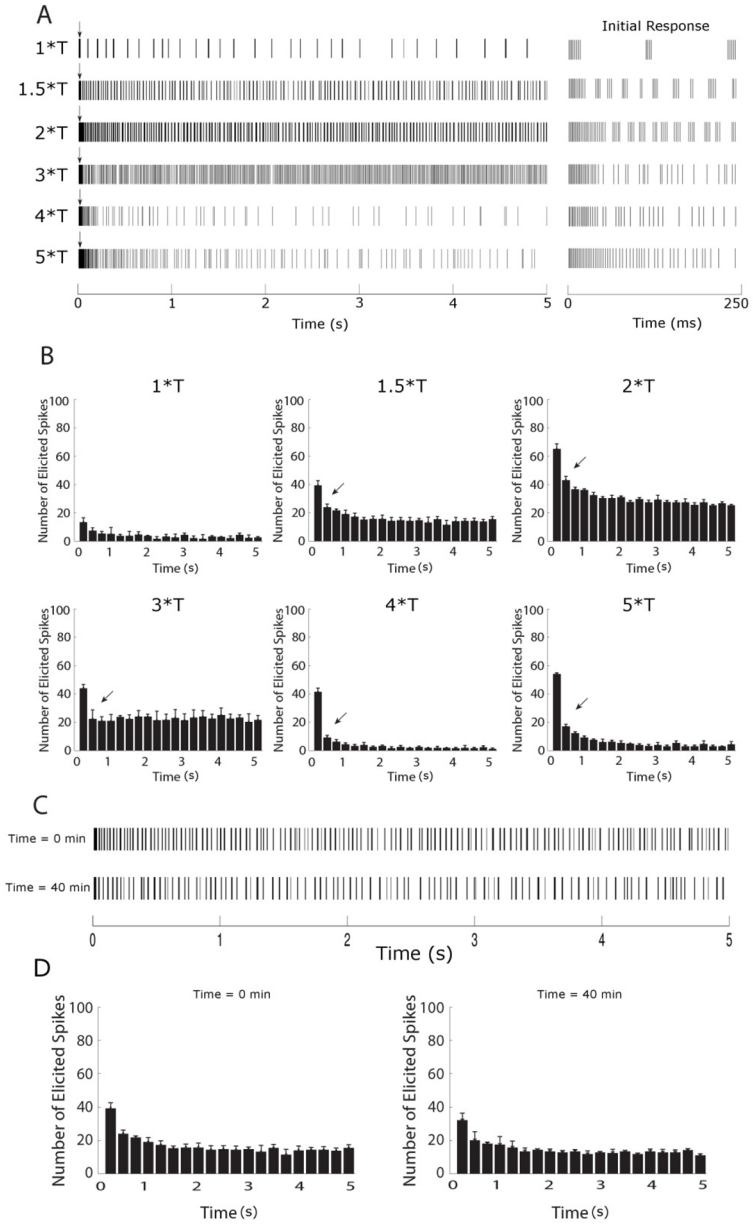

Figure 2.

Brisk-transient cells are sensitive to stimulus amplitude at 2000 PPS. (A) Spike rasters of the full 5 second response (left) and the initial 250 ms of the response, shown in expanded scale (right), of an OFF-BT cell to 2000 PPS stimulation at the amplitude levels indicated on left (T = 17 μA, see text); all responses are from the same cell. Each vertical line represents a single spike; bursts of spikes appear darker. A brief period of elevated spiking (arrows) was observed at the beginning of all trials. (B). Histograms of the spike trains in (A); Bin sizes were 250 ms and each histogram represents the average of 3 trials. (C) Response to 1.5*T pulse train at the beginning of an experiment (top) and the response to the identical stimulus 40 minutes later (bottom). (D) Histograms of the early and late responses in (C) reveal no significant differences between responses over time.

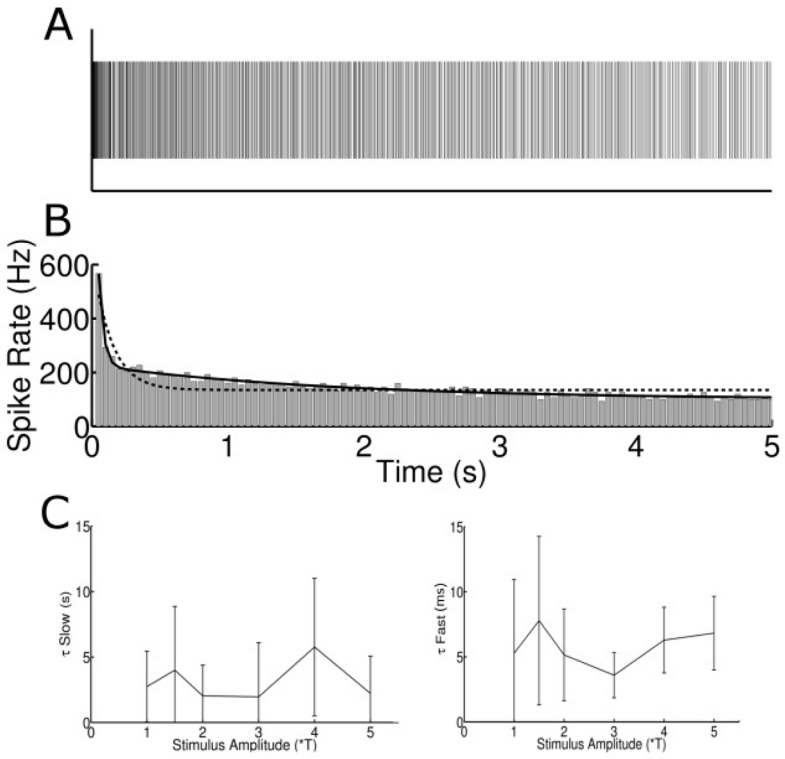

Figure 3.

Responses desensitize in two phases. (A) Typical spike raster to 3*T stimulus. (B) Histogram of the spike raster in (A). Bin size: 50 ms. Bin heights were fit with a single exponential curve (dotted line) as well as a double exponential (solid line). (C) The time constants for the slow (left) and the fast (right) component of the double exponential equation as a function of stimulus amplitude for all cells. Error bars represent ± SD

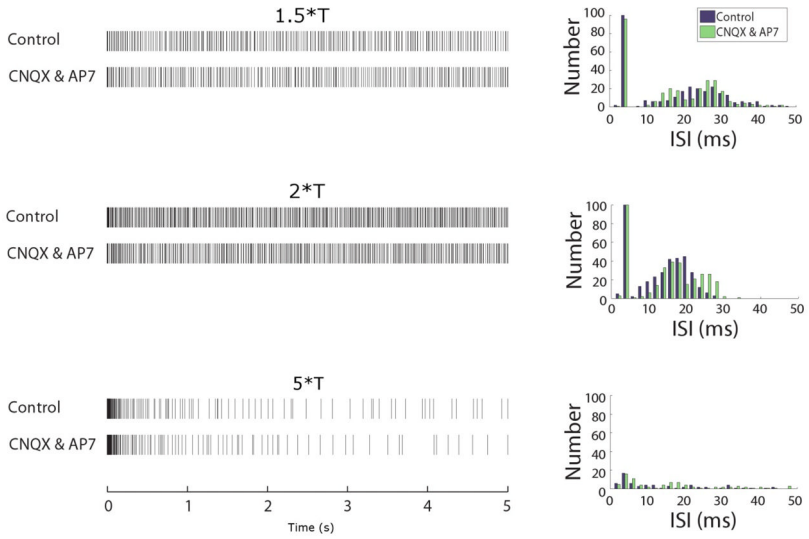

Figure 4.

Responses to 2000 PPS stimulation are mediated through direct activation. Spike rasters (left) in control conditions (top rows) and after the application of the synaptic blockers CNQX and AP7 (bottom rows) to the bath. Right panels contain histograms of the ISIs from each raster pair (control and drug).

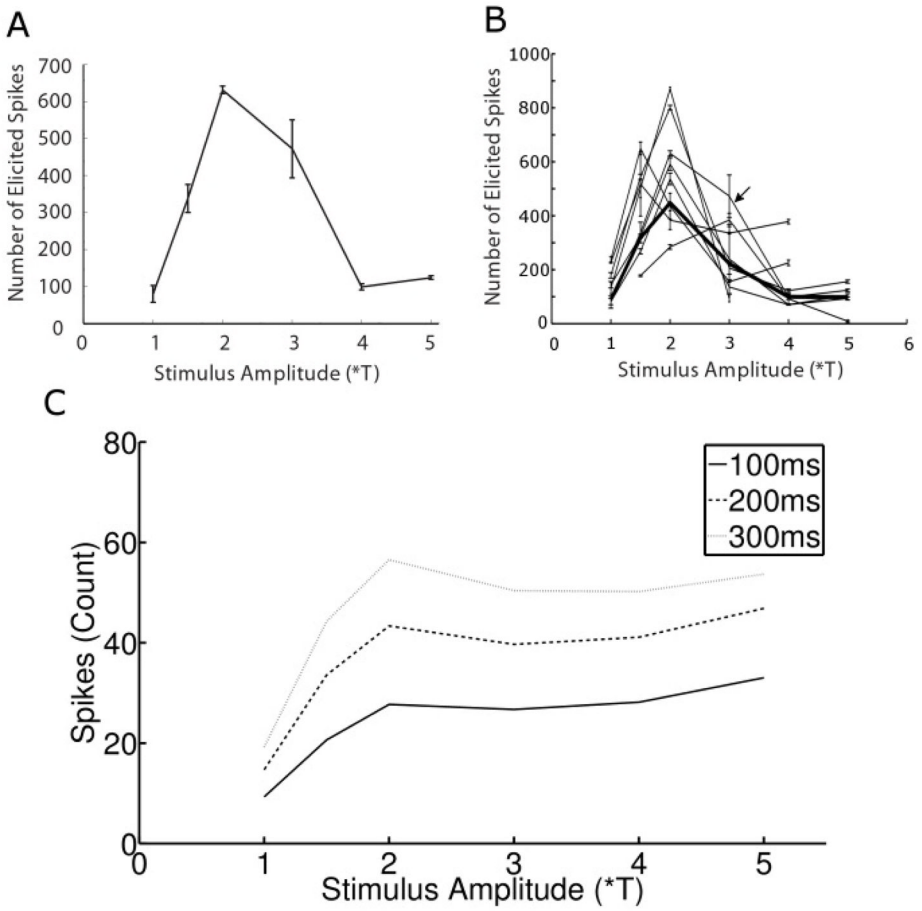

Figure 5.

Response sensitivity to amplitude is bimodal. (A) Total number of elicited spikes as a function of stimulus amplitude for a typical OFF-BT cell. Each point is the average of three trials, and error bars show standard deviation. (B) Overlay of similar amplitude sensitivity plots for all cells; arrow indicates the cell in (A). Thick line: average of responses from all cells. (C) Spike counts were determined for time intervals following stimulus onset of 100ms (dark line), 200ms (dashed line) and 300ms (light line).

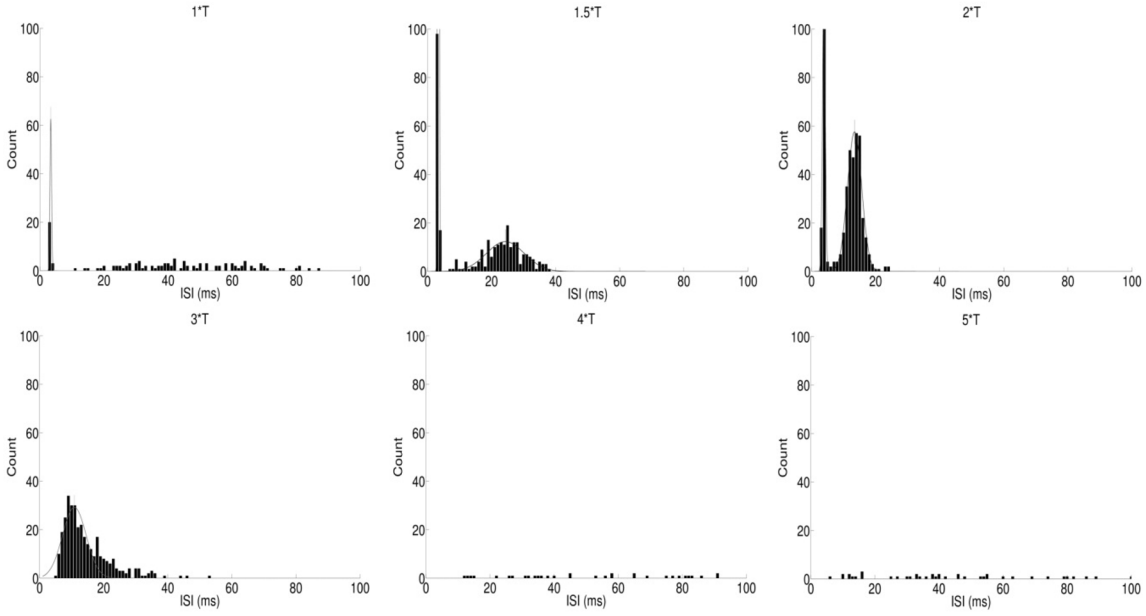

Figure 6.

Inter-spike interval histograms. ISI histograms were determined for the response to six different amplitudes. Each peak was fit with a separate Gaussian curve (thin solid lines). Only spikes that occurred ≥ 250 ms after stimulus onset were analyzed (see text).

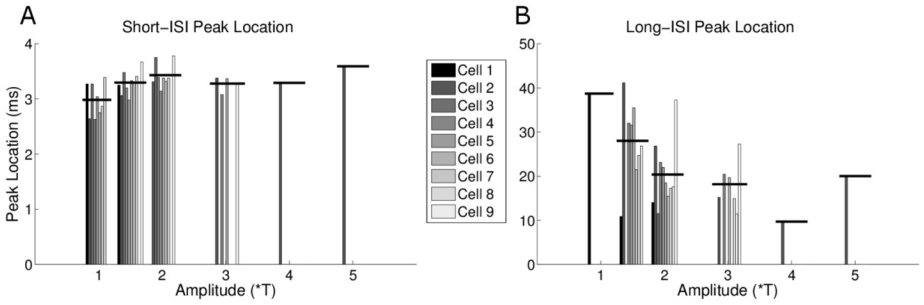

Figure 7.

Burst properties are amplitude sensitive. (A) Short-ISI peak location clustered by stimulus amplitude. Each bar represents the location of the center of the Gaussian fit for an individual cell (see figure 6). (B) Long-ISI peak location. The black horizontal lines represent the mean location for each amplitude level.

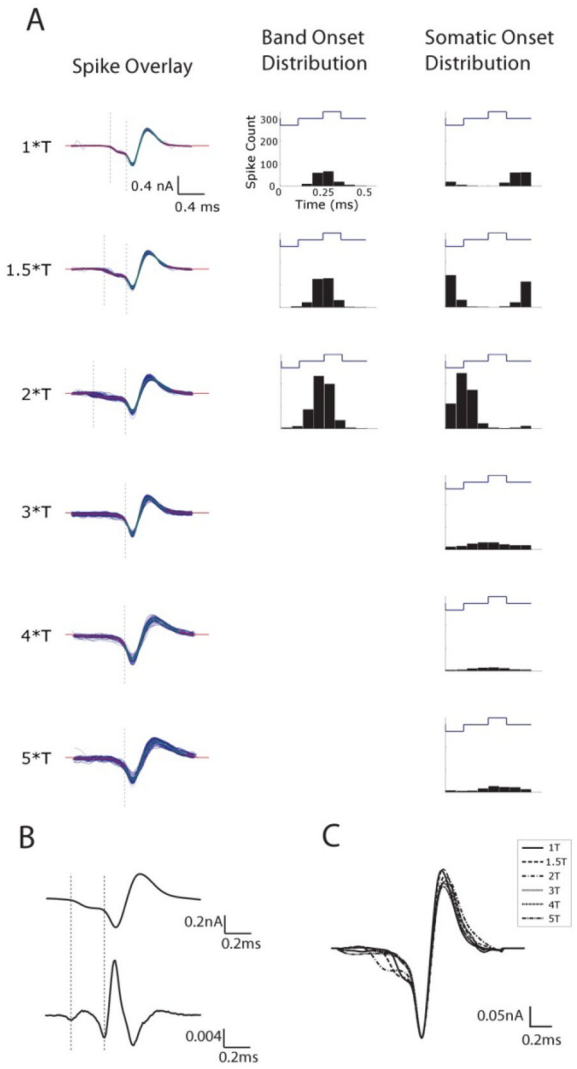

Figure 8.

Spike kinetics are altered by stimulus amplitude. (A) (Left column) Overlays of all extracted spikes from a single trial at each amplitude. Amplitudes of 1, 1.5, and 2*T exhibited two separate depolarization phases: a small depolarization (onset indicated by left dotted lines) followed by a large depolarization (onset indicated by right dotted lines). Amplitudes greater than 2*T exhibited only a single depolarization phase. (Middle column). Peri-stimulus time histogram (PSTH) of the onset of the small depolarization relative to the phase of the stimulus waveform. (Right column) PSTH of the onset of the large depolarization relative to the phase of the stimulus waveform. (B) Onsets of small and large depolarizations were determined by calculating the local minima associated with the second derivative (bottom) of each waveform. (C) Overlay of spike kinetics from all amplitudes reveals timing differences as a function of stimulus amplitude.

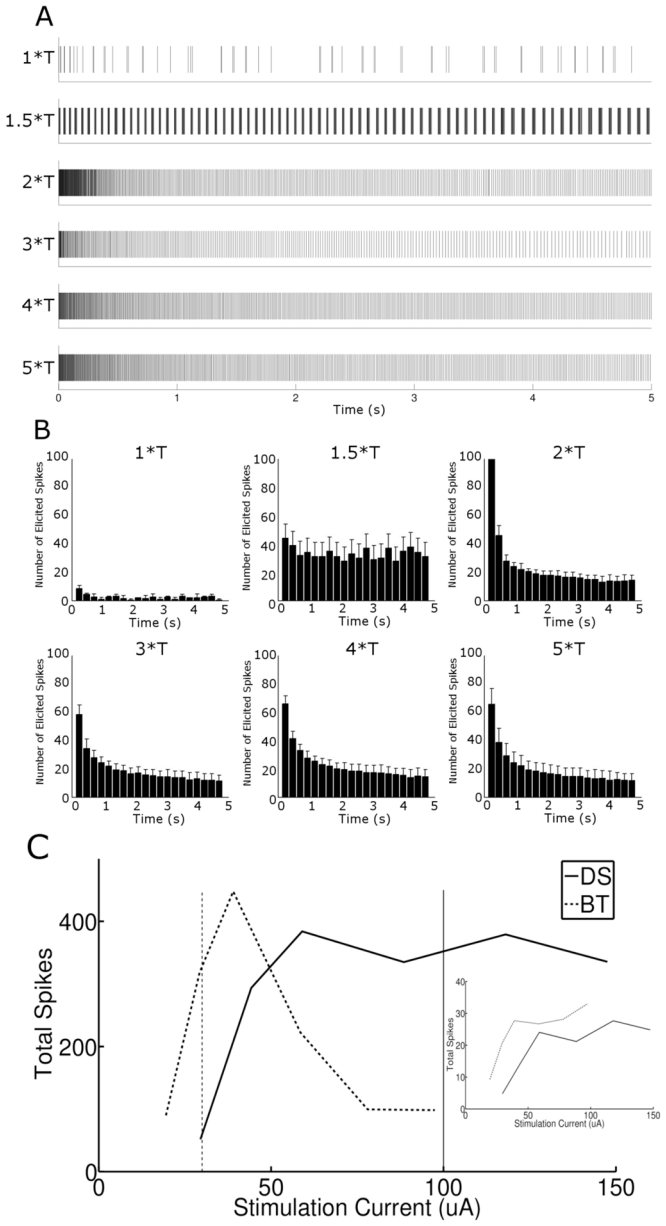

Figure 9.

Response of directional selective ganglion cells differs from OFF-BT responses. (A) Spike rasters of a single DS cell in response to stimulation at different amplitudes (levels indicated at left). (B) Histograms of spike trains in (A). Bin size was 250 ms, and each plot is the average of 3 trials. (C) Total number of spikes across 5 second trials averaged over all trials and all cells (DS N = 6, OFF-BT N = 9). Inset compares total spikes in the first 100ms ('initial' response) for DS and BT cells.

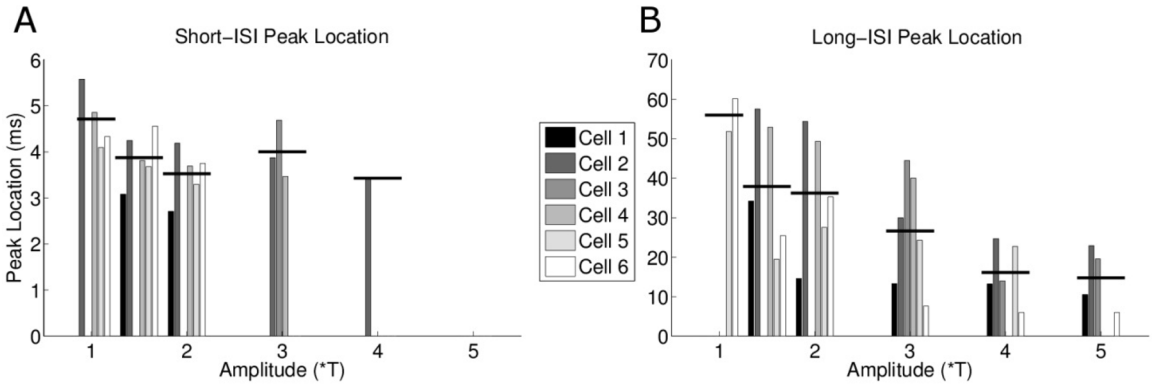

Figure 10.

ISI analysis of burst spiking in DS Cells. (A) Short-ISI peak location clustered by stimulus amplitude. Similar to Figure 7, each bar represents the center peak location of the Gaussian fit (see figure 6); horizontal bars represent the mean ISI at each amplitude level. (B) Same as (a), except for long-ISI peak locations.